Energy Equip. Sys./ Vol. 11/No. 2/June 2023/ 231-246

ENERGY EQUIPSYS

Energy Equipment and Systems
http://energyequipsys.ut.ac.ir
www.energyequipsys.com

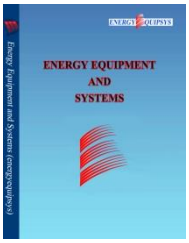

Effect of fire location on the smoke temperature and CO distributions in a subway tunnel with train carriages: A numerical study

Authors

Amin Khodadadi Behtash [a]*
Seyed Esmail Razavi [a]

[a] Faculty of Mechanical Engineering, University of Tabriz, Tabriz, Iran

Article history:

Received : 31 January 2023
Accepted : 23 March 2023

ABSTRACT

In this study, a numerical simulation of the full-scale train with four carriages is considered, and different fire scenarios on the subway tunnel floor are performed in terms of fire locations and heat release rate variations. The subway tunnel is longitudinally ventilated, where vertical temperature stratification and carbon monoxide (CO) are determined at the mid-line of carriages by a fire-dynamic simulator (FDS). Also, fire-hazardous conditions are reported by under-ceiling sensors inside the carriages. The results show that both first and second carriages experience high temperature and CO concentration of smoke flow when the nearest fire location to the carriages is assumed with a fixed fire heat release rate of 10MW (HRR). By changing the fire location in the tunnel, the unsafe situation of the first carriage is reported for two different fire source locations.

Keywords: Heat Release Rate of Fire, Fire Location, Train Carriages, Temperature Distribution.

1. Introduction

The subway is recognized as an effective means to handle transport problems in congested cities; thus, many subway lines are built and operated worldwide. Despite the convenience, great capacity, and less pollution of subway systems, their drawbacks, such as tunnel fire, accidents, explosions, and train derailments [1-4], are the main factors for engineers to cope with different scenarios in a metro system. Metro train fire has been extensively discussed in the literature [5-6]; Carbon Monoxide distribution is the main reason for deaths in 85% of cases [7]. Therefore, it is necessary to report the temperature stratification and toxic smoke products, such as Carbon Monoxide, distribution for different subway fire scenarios. Smoke stratification under the ceiling, fire source features, and ventilation modes have been studied by many researchers [8-10]. For instance, Cong et al. [11] studied train fire location on the maximum temperature of smoke under tunnel ceiling both numerically and theatrically. They considered fire location inside 3 train carriages and inspected the relation between spill plume (through doors) and smoke temperature; they then modified the maximum temperature under the tunnel ceiling with various fire sizes and locations. Further, Peng et al. [12] studied carriage fire and temperature profiles under the ceiling and different doors. Their experiments showed that as longitudinal distance increased from the source temperature, the gradient under the ceiling decreased. Also, they reported the effect of door status on ceiling temperature.

* Corresponding author: Amin Khodadadi Behtash
Faculty of Mechanical Engineering, University of Tabriz, Tabriz, Iran
Email: amin.behtash@gmail.com

Ceiling smoke temperature distribution in a subway train involving various fire locations and door statuses was considered by the reduced-scale subway train model in Peng et al. [13]. They found a novel empirical model for longitudinal and transverse ceiling smoke temperature in the subway train model. Meng et al. [14] conducted experiments in a reduced-scale model (1:10) of the subway station. They analyzed the maximum smoke temperature and the longitudinal temperature distribution under the tunnel ceiling with two types of conjunction doors between the platform and tunnel. Results indicated that the heat release rate of fire and door types had major effects on the under-ceiling temperature of smoke flow. Weng et al. [15] carried out full-scale experiments and numerical simulation using FDS 5.5 in a tunnel with one end joined to a metro station to investigate smoke control efficiency and longitudinal temperature distribution with different fire HHRs, oil pan sizes, and four different operation modes for emergency vents. The main results showed the faster velocity of smoke spread toward the station compared to the tunnel opening entrance. Lei et al. [16] studied the impact of different fire source positions on a subway station environment. They found two critical evacuation modes among various cases of simulation. Yuan et al. [17] investigated the effect of train location, fire source in carriages, and carriage fire in trains on the smoke temperature beneath the ceiling using FDS as the CFD code. The results revealed the fire source location and the carriage fire in the train to have a significant effect on the under-ceiling smoke temperature. Ji et al. [18] conducted a simplified calculation technique on the maximum temperature beneath the ceiling in subway station fires. They found that maximum smoke temperature growth was not much influenced by the location of fire longitudinally Sojoudi et al [19] numerically used a large eddy simulation (LES) to predict the vertical carbon monoxide concentration and temperature distribution in a tunnel with different locations of the fire source. Both the vertical gradients of CO concentration and smoke temperature have decreased with the velocity rise. They also discussed carbon monoxide distribution and temperature vertical distribution in case of tunnel fires [20-22]. They mentioned vertical values of CO distribution which is important to find the out thickness of the smoke where one can be aware of smaller thickness for a higher aspect ratio. Their result is that obtained CO decay velocity is faster than temperature values [21].

Shan-Jun et al. [23] studied the fire smoke hazard in a carriage numerically by FDS. After 100 s, the results further showed the effect of hazardous parameters, such as temperature rise, CO concentration, visibility, and smoke sinking.

Recently, the study on train fire accidents in metro tunnels has been discussed in terms of fire location, maximum smoke temperature, fire accident, smoke control, platform screen doors, emergency ventilation, blockage effect, multi-window carriages, and tenability of the passengers [24-29] Fire distance is considered as a controlling parameter [27]. In addition, Cong et al [27] studied the variation of ceiling gas temperature in a subway train with different fire locations. In their numerical results, the importance of fire location and heat release rate have been highlighted. They stated that the ceiling gas temperature rise is affected by the pressure difference on both sides of the fire source and the backflow from the end wall, which depends on the heat release rate and the fire location. Ren et al [30] conducted a series of full-scale numerical simulations under the condition of a double fire source with a metro train in the tunnel to study temperature distribution and maximum temperature rise. It is found that the longitudinal temperature distribution of tunnel fire smoke is still exponentially decreased under different fire source separations. This study investigates the fire location and HRR inside a train with four carriages and the fire source outside the train on the tunnel floor. Smoke temperature and CO distribution are determined under the ceiling of each carriage to distinguish unsafe carriage. In all models mentioned in earlier studies, tunnel fire with several carriages has not been discussed for hazardous conditions defined with the train under-ceiling temperature distribution and CO concentration. The paper also focuses on the vertical distribution of the aforementioned parameters to address the harmful situations in the carriages. Fire-dynamic simulator 6.6 is adopted to develop a CFD code to evaluate the

different scenarios of simulation. The following are the key goals of this paper:

- The ability to identify the carriage number with hazardous conditions during fire ignition on the tunnel floor.
- To achieve vertical temperature and CO distribution of carriages.
- Finding the precise temperature and CO concentration at the mid-point of the carriage through time.

Nomenclature

Specific heat capacity, kJ. kg^{-1}. K^{-1}	C_p
Diffusivity coefficient, m^2. s^{-1}	D
Length characteristic of the cell, m	D'
External force vector, kg.m.s^{-2}	f
Froude number	Fr
Gravity acceleration, m.s^{-2}	g
Enthalpy, kJ	h
Tunnel height, m	H
Heat release rate, kW	HRR
Thermal conductivity, W .m^{-1}. K^{-1}	k
Turbulent thermal conductivity, W .m^{-1}. K^{-1}	k_t
Pressure, Pa	p
Turbulent Prandtl number	Pr_t
Heat released from fire, kW	Q
Radiative flux, kW.m^{-2}	q_r
Heat release rate per unit volume, kW.m^3	$\dot{q}'''$
Turbulent Schmidt number	Sc_t
Time, s	t
Temperature, °C	T
Ambient temperature, °C	T_a
Velocity vector, m.s^{-1}	u
Mean velocity, m.s^{-1}	$\bar{u}$
Mass fraction of species	Y
Mass fraction of fuel	Y_i
Mass fraction of fuel with fire	Y_l
Mixture fraction	Z
Dissipation rate of turbulence	ε
Density, kg .m^{-3}	ρ
Ambient density, kg.m^{-3}	ρ_a
Traveling smoke layer density, kg.m^{-3}	ρ_s
Turbulent viscosity, kg. m^{-1}. s^{-1}	μ_t
Viscous stress tensor, kg.m.s^{-2}	τ
Velocity vector, x-axis direction, m.s^{-1}	u_{ijk}
Velocity vector, y-axis direction, m.s^{-1}	v_{ijk}
Velocity vector, z-axis direction, m.s^{-1}	w_{ijk}
Filter width in LES, dimensionless	Δ
Grid size in the y-direction, m	δy
Grid size in the x-direction, m	δx
Grid size in the z-direction, m	δz

2. Definition of physical model

The subway tunnel for the present study is shown in Fig. 1 (a) with a typical size of $300m \times 5m \times 5m$ (length, width, height) and a side view of the tunnel with train blockage in Fig.1 (b). Four train carriages [31] are considered in the subway tunnel with a total size of $100m \times 2.5m \times 3m$. Each carriage has 4 doors and 5 windows. Doors are located at each side of carriages with a dimension of 1.4m wide $\times$ $24m$ high, and windows with a dimension of 0.7 m wide $\times$ $1m$ high (see Fig. 1 b, c and d). A fire source is considered at the centerline of the subway tunnel. The "BURNER" size is $1m \times 1m \times 1m$, and propane is used as fuel for the fire source with default values of the FDS user Guide [32]. The distance of sensors throughout the carriages is 0.33 m, illustrated by red dots in Fig. 1. A series of sensors are located beneath the ceiling 0.1 m to determine the temperature and CO concentration variations.

In all cases, the ambient temperature is 25 ℃, and the pressure is 101.325 kPa. Different heat release rates of the fire source are selected as 2.5 MW, 5 MW, 7.5 MW, and 10 MW for multiple scenarios. The fraction of fuel mass converted into a smoke particle, y_s, is fixed at 0.1 [33]. In the LES simulations by FDS, the default radiative fraction is 0.35.

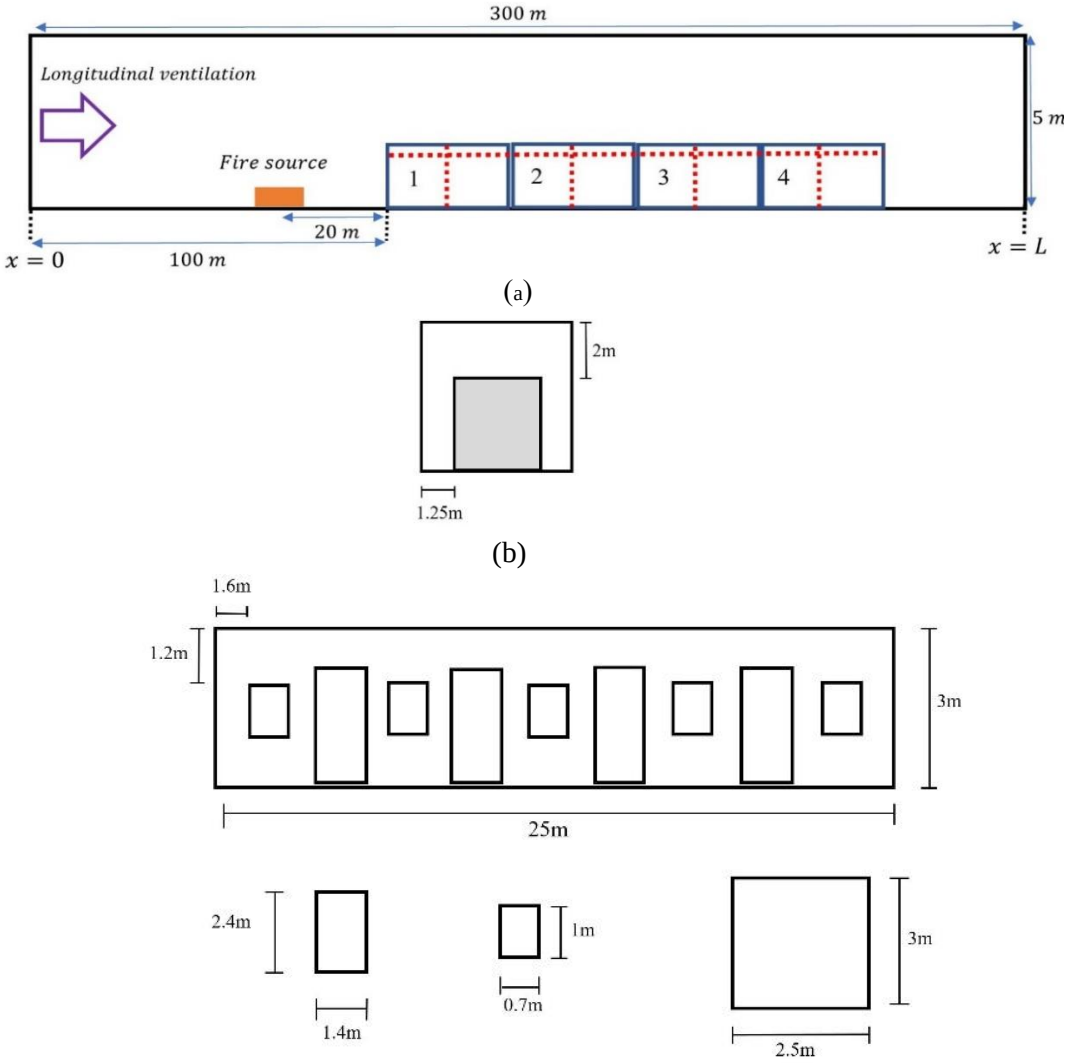

Fig. 1 (a) Schematic view of the subway tunnel with carriages and sensor locations (red colored); (b) Side view (b) Carriage model [31]; (c) Dimensions of doors and windows; (d) Cross-sectional area

. The specified boundary conditions of the walls, floors, and ceilings of the subway tunnel are thermally thick. The material properties of tunnel walls are set as "concrete," and train carriages are made of "steel." These materials and related thermal properties are presented. (Table1).

The boundary condition for the left portal is assigned to be an air "SUPPLY" vent to attain a fixed longitudinal ventilation velocity of 1 m/s, and it is considered as an "OPEN" boundary for the right side. All boundary conditions are stated mathematically as below:

Table 1 The thermal properties of the material [22]

Model	Material	Thickness (m)	Density (kg/m^3)	Specific heat $(kJ/(kgK)$	Conductivity $(w/(mK))$
walls	Concrete	0.3	2280	1.04	1.80
Carriages	Steel	0.1	7850	0.46	45.8

Momentum and energy:

Supply condition: $u = 1m/s,\ v = 0,\ w = 0$

Open condition: $p = p_{atm}$

No slip velocity and thermally thick condition:

$$side\ walls: \partial u/\partial y = 0, \partial u/\partial z = 0,\ \partial T/\partial y = 0$$

$$ceiling: \partial u/\partial y = 0, \partial u/\partial z = 0,\quad \partial T/\partial z = 0 \tag{1}$$

Species:

Supply condition: $Y_i = 0\ D_i = 0,\ Z_i = 0$

Open condition: $p = p_{atm}$

No diffusive condition:

$$side\ walls: \partial Y_i/\partial y = 0, \partial Y_i/\partial z = 0,\ \partial D/\partial y = 0, \partial Z_i/\partial y = 0,$$

$$ceiling: \quad \partial Y_i/\partial y = 0, \partial Y_i/\partial z = 0,\quad \partial D/\partial z = 0, \partial Z_i/\partial z = 0, \tag{2}$$

Simulations are performed for 240 seconds, which is sufficient to distribute the smoke spread at the tunnel [34]. In all simulations, the train is assumed to be stopped in the tunnel. In order to simplify the model, all doors and windows are supposed to be open [22]. Also, the simulated layout of the subway tunnel model with the train compartment is shown (Appendix Fig (a)).

3. Governing equations and solution method

A numerical simulation is conducted using the Fire-Dynamic Simulator developed by the National Institute of Standards and Technology (NIST) [36]. The basic governing equations for subway tunnel fire, including continuity, momentum, energy, and conservation of species [2], are expressed by:

$$\frac{\partial \rho}{\partial t} + \nabla.\rho u = 0 \tag{3}$$

$$\frac{\partial}{\partial t}(\rho u) + \nabla.\rho uu + \nabla.p = \rho g + \nabla.\tau \tag{4}$$

$$\frac{\partial}{\partial t}(\rho u) + \nabla.\rho uu + \nabla.p = \rho g + \nabla.\tau \tag{5}$$

$$\frac{\partial}{\partial t}(\rho Y_i) + \nabla.\rho Y_i u = \nabla.\rho D_i \nabla Y_i \tag{6}$$

where ρ is the density, u represents the velocity vector, g is the gravity acceleration, p is the pressure, h is the enthalpy, $\dot{q}''$ shows the conductive and radiative heat fluxes, $\dot{q}'''$ is the heat release rate per unit volume, Y_i is the mass fraction of species i, D_i is the diffusion coefficient of species i, ε is the dissipation rate, and τ , as given below, is the stress tensor:

$$\tau = \mu\left(2S_{ij} - \frac{2}{3}\delta_{ij}(\nabla.u)\right);$$

$$S_{ij} = \frac{1}{2}\left(\frac{\partial u_i}{\partial x_j} + \frac{\partial u_j}{\partial x_i}\right) \quad i.j = 1.2.3;\ \delta_{ij} = \begin{cases} 1 & i = j \\ 0 & i \neq j \end{cases} \tag{7}$$

FDS introduces the large-eddy simulation as a turbulence modeling technique to provide second-order accurate numerical space differences [35]. Time integration of flow variables is performed with an explicit second-order predictor-corrector scheme. The sub-grid scale turbulence modeling is defined as Smagorinsky in FDS. Viscosity, $\mu_{t,}$ is modeled by the Smagorinsky analysis as

$$\mu_t = \rho(C_s\Delta)^2\left(2\bar{S}_{ij} : \bar{S}_{ij} - \frac{2}{3}(\nabla.\bar{u})^2\right)^{\frac{1}{2}}, \tag{8}$$

where C_s is the Smagorinsky constant, and Δ is defined as length on the order of grid cell size. Theoretically, C_s is set equal to 0.17 in fire scenarios [35], which can alter in the range of 0.1 to 0.25 for different applications. $\bar{S}_{ij}$ denotes the symmetric rate of strain tensor as

$$\bar{S}_{ij} = \frac{1}{2}\left(\frac{\partial \overline{u_i}}{\partial x_j} + \frac{\partial \overline{u_j}}{\partial x_i}\right). \tag{9}$$

Thermal conductivity and material diffusivity are correlated to the turbulent viscosity, $\mu_{t,}$ via

$$k_t = \frac{\mu_t C_p}{Pr_t}, \tag{10}$$

And

$$(\rho D)_{l.t} = \frac{\mu_t}{Sc_t}, \quad (11)$$

where Pr_t is turbulent Prandtl number, and Sc_t represents Schmidt number. Both of these parameters are assumed equal to 0.5 in all scenarios [35]. The combustion model of mixture fraction theory is admitted for large-eddy simulation in FDS. The mixture fraction is stated by $Z(x.t)$, and it relates to the conservation equation by[32]

$$\rho \frac{dZ}{dt} = \nabla.\rho D \Delta Z. \quad (12)$$

4. Grid sensitivity and validation

It is well known that simulation results can be affected by grid size sensitivity in FDS. Therefore, in this study, the grid size is evaluated to achieve the desired reliability in predicting results. As suggested by McGrattan et al. [35], the grid size near the fire source is declared by $D'/\delta x$ in the range of 4 and 16. This limitation can ensure acceptable simulation results. D' represents the characteristic diameter of the fire source a given by

$$D' = \left(\frac{Q}{\rho C_p T_a \sqrt{g}} \right)^{2.5}, \quad (13)$$

where Q is the heat release rate of fire, T_a is the ambient temperature, ρ is the air density, C_p is the air-specific heat, and g is the gravity acceleration. For this study, the mentioned grid size of the fire source vicinity is 8.90 for 10MW fire HRR, being acceptable due to the range.

Better resolution of the simulation results can be expected in FDS analyses while the spanning cells of the fire region are smaller. Furthermore, grid size must be smaller than $0 \cdot 1D'$ to attain reliable numerical results. The smallest grid size in the subway tunnel is 0.125 m in the simulations, leading to dependable numerical results. The finer and coarser regions of mesh sizes are listed (Table 2).

The time step and convergence criteria are limited by Courant-Fredrich-Lewy (CFL) condition in FDS [23] as

$$\delta t \max \left(\frac{\left(\left|u_{ijk}\right|\right)}{\delta x}, \frac{\left(\left|v_{ijk}\right|\right)}{\delta y}, \frac{\left(\left|w_{ijk}\right|\right)}{\delta z} \right) < 1, \quad (14)$$

where δx, δy, and δy represent the size of the smallest grid cell in x, y, and z directions, respectively. During the simulation process in FDS, the time step varies to guarantee the CFL condition. Figure 2 shows maximum CFL number during FDS simulation for the subway under 10 MW fire with train carriages. The CFL convergence criteria of subway simulation varies in a range of 0.73 to 0.98 throughout the iterations. The time step size is adjusted automatically in a range of 0.0018- 0.0041s by FDS during subway fire simulation.

Table 2. Grid sizes for the sensitivity study

Grid system	Grid size inside the carriages (m)			Grid size in subway tunnel (m)		
	δx	δy	δz	δx	δy	δz
A	$0 \cdot 125$	$0 \cdot 125$	$0 \cdot 125$	$0 \cdot 20$	$0 \cdot 20$	$0 \cdot 20$
B	$0 \cdot 125$	$0 \cdot 125$	$0 \cdot 125$	$0 \cdot 25$	$0 \cdot 25$	$0 \cdot 25$
C	$0 \cdot 125$	$0 \cdot 125$	$0 \cdot 125$	$0 \cdot 30$	$0 \cdot 30$	$0 \cdot 30$
D	$0 \cdot 125$	$0 \cdot 125$	$0 \cdot 125$	$0 \cdot 45$	$0 \cdot 45$	$0 \cdot 45$
E	$0 \cdot 125$	$0 \cdot 125$	$0 \cdot 125$	$0 \cdot 60$	$0 \cdot 60$	$0 \cdot 60$

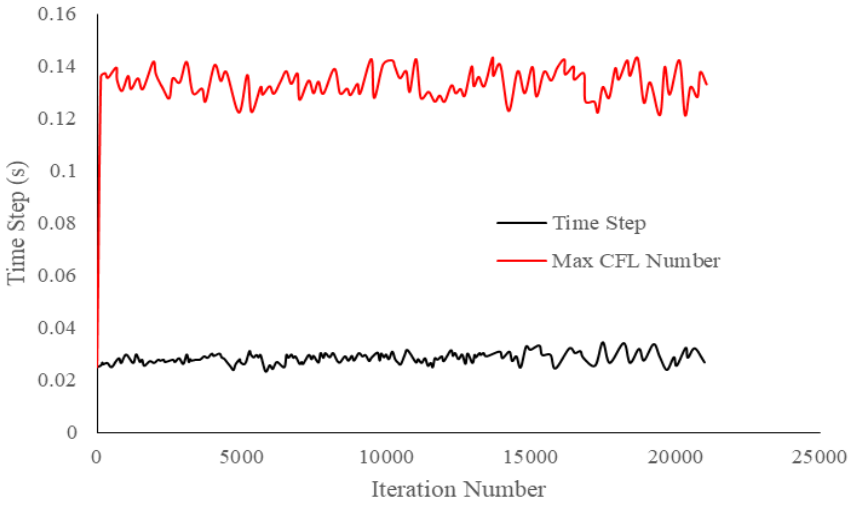

Fig. 2 Time step and maximum CFL number variations during FDS simulations

As shown in Fig. 3, longitudinal temperature distribution change of smoke is observed beneath the subway tunnel ceiling under 10 MW fire. There is no significant change in temperature distribution for grid systems A and B. Further, as seen in this figure, differences in temperature profiles are shown in magnified form in the circle, indicating the trivial difference between grid systems A and B. The average difference in temperature profile data for both mentioned grid systems is 1.4%. Thus, grid system B is adopted for all scenarios considering fewer mesh cells and taking much less computational time compared to grid system A.

Vertical distribution of the mean velocity for different grid systems at mid line of the tunnel is shown (Appendix Fig. (b)). Temperature value usually behaves very adaptable with the mesh size. Therefore, the test of vertical distribution of the mean velocity is plotted. Grid size A with 914256 cell number has the nearest value of velocity with grid size B with 1238680 cell number The validation process is completed by comparing Gao's experimental study [37] with 120kW fire HRR for model scale and 3.16 MW for full scale. He has found maximum smoke temperature and longitudinal decay in a horseshoe-shaped tunnel fire. Also, Cong et al. [11] have compared their results with those of Gao's study. At present simulation, Fig. 4 shows the ceiling temperatures calculated by FDS of a similar case to the previous studies [11, 37]; it is in line with the experimental and theoretical data indicating FDS capability in tunnel fire simulations.

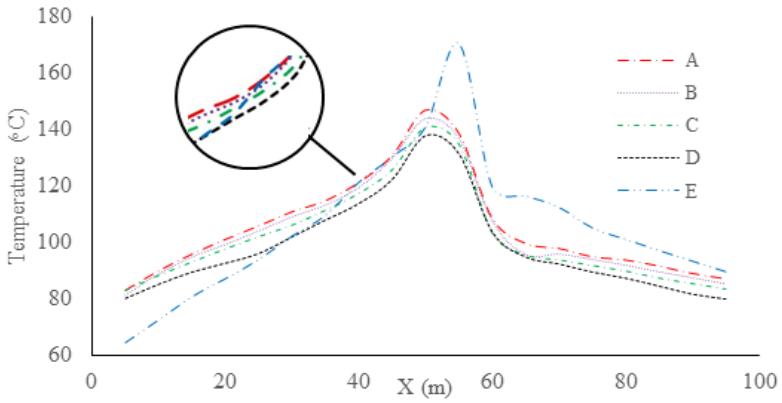

Fig. 3. Longitudinal temperature profile under the subway tunnel ceiling for different grid systems

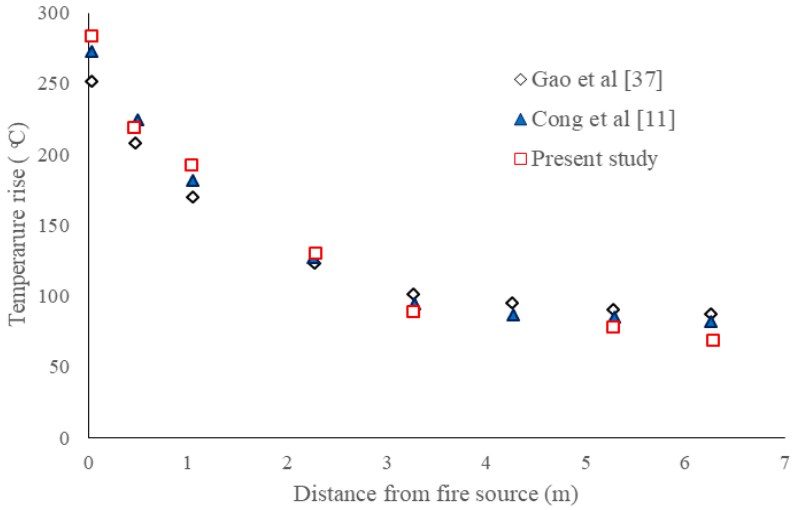

Fig. 4. Comparison of temperature rise beneath the tunnel ceiling

5. Results and discussion

Simulation results are divided into 3 distinct sections, including the considerations of carriage number, fire location effects, and HRR effects. The vertical profiles of temperature and CO distribution are plotted for all 4 carriages particularly. All the simulation cases are reported (Table 3). To evaluate the different scenarios of simulation, critical values of passenger's tenability inside the carriages are assumed as 80°C (temperature) and 2000 ppm for Carbon Monoxide concentration.

Table 3 All cases of simulations by FDS for the present study

Case	Fire HRR (MW)	Fire location (m)
1	2.5	80
2	5	80
3	7.5	80
4	10	20
5	10	40
6	10	60

5.1. The consideration of carriage number

Figure 5 shows the vertical temperature change in different carriages at the center line of each for the fixed fire distance. As seen, the farther the carriage from the fire source, the less vertical temperature is determined; this is due to the heat loss through the carriage walls and openings such as doors and windows. Also, it can be inferred that the first and second carriages show the hazardous temperature under the ceiling. Moreover, the vertical temperature profile is ascendant as height increases in carriages. The third and fourth carriages experience lower temperatures as heat losses increases by train compartment.

Vertical velocity profile of carriages is a vital factor for controlling hazardous conditions of tunnel fire. Fig. 6 shows the vertical profile of CO concentration in the fixed fire position in different carriages. Higher values of CO concentration are shown in carriage numbers 1 and 2. CO concentration increases with height since smoke density is lower than air density; carriage doors and windows help dilute hazardous species by fresh airflow at lower heights. Velocity rises as height increases at all carriages; however, a trivial velocity change is observed among carriages, (Appendix Fig (c)).

Open doors and windows of each carriage have significant effect on the diluting the smoke toxicity and temperature at lower heights of carriages. The blockage effect of carriages leads to larger velocities throughout the tunnel, improving the mixing effect of smoke layers in the vertical direction. Thus, the temperature decay in the vertical direction from the ceiling to the floor is due to velocity variations.

5.2. The consideration of fireplace

As the fire gets near the carriage, higher temperature distribution under the ceiling is reported. Dangerous temperature conditions are shown for the fireplaces of 60 and 80 meters away from the tunnel entrance. In comparison, the carriage untenable temperature for passengers is not reported for lower heights which are the same for all fire distances. The fire location effect on the vertical temperature distribution inside a specific carriage are shown (Appendix Fig (d)).

The distribution of vertical CO content and vertical velocity is highly related together. Smoke velocity is the main reason of CO concentration variation at the middle height of carriages. Indeed, a small increase in the velocity reinforces the smoke flow to move faster, and dilution of harmful species is well enhanced. Higher CO concentration for different fire positions to the carriages is plotted (Appendix Fig (e), Fig (f)).

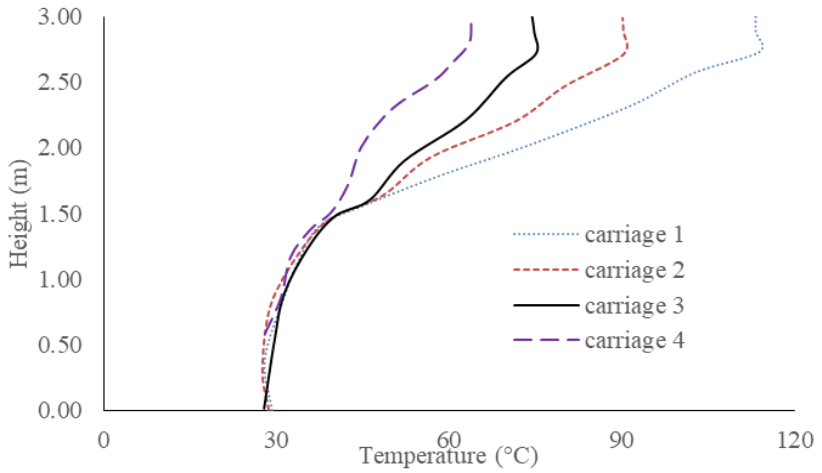

Fig. 5. Vertical temperature variations in the fixed fire position

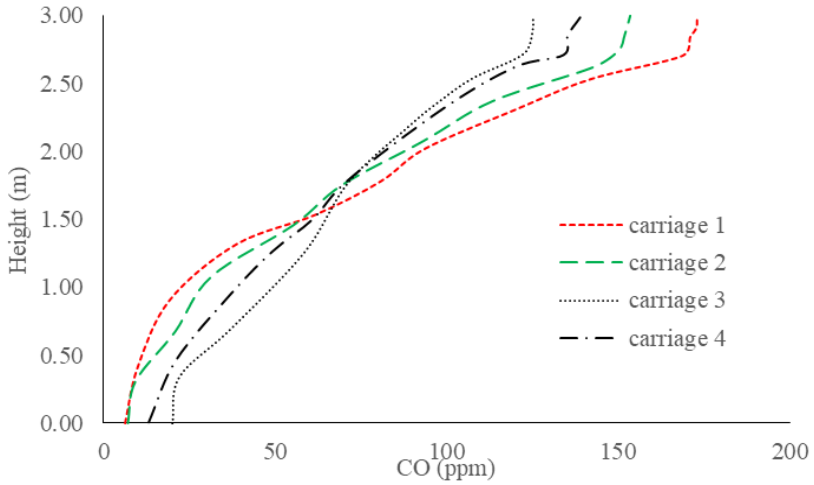

Fig. 6. Vertical CO concentration in the fixed fire position

5.3. The consideration of HRR through simulation period

To better assess the HRR's effects on the under-ceiling temperature distribution and CO concentration along the train carriages, these parameters' profiles are shown versus time. Simulation time is not only a triggering factor for smoke propagation in the subway tunnel fires but also influences the hazardous conditions in the train compartment. In this section, HRR change measurements are discussed. As seen in Fig. 7, the under-ceiling temperature rises with HRR increment. The figure also illustrates that two big HRRs of 7.5 and 10 MW are responsible for unsafe conditions after 150 and 110s. In this regard, the reported critical temperatures are 101.6 ℃ and 113.2℃. The temperature increases of higher HRRs attribute to buoyancy-driven flow effects of the smoke movement and heat convection inside the carriages. During the simulation time, Fire HRRs of 2.5 and 5 MW have not considerable effect on the under-ceiling temperature at each carriage.

In Fig. 8, carbon monoxide variations with HRR change indicate that the concentration of toxic species beneath the ceiling increases with the growth of HRR versus time. In this simulation, it is better to declare that CO concentration is not the controlling mechanism of life-threatening conditions inside the carriages while its concentration is below the critical passenger's tenability.

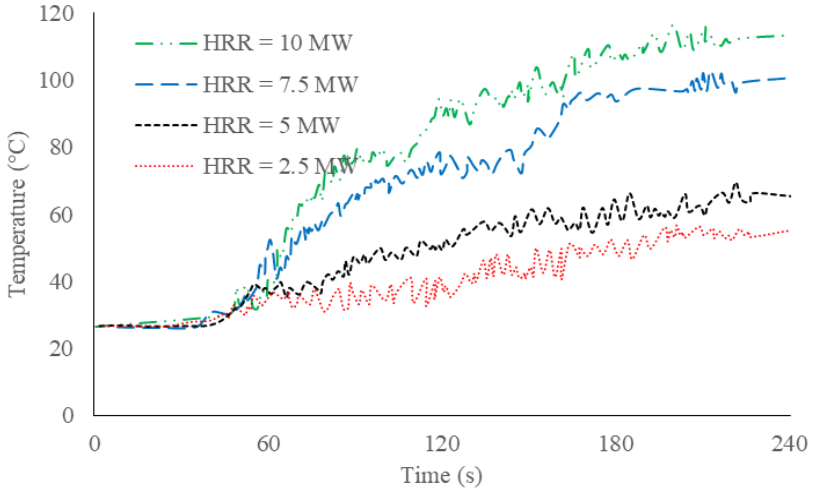

Fig. 7. Temperature variations vs. time under the carriage ceiling for different HRRs

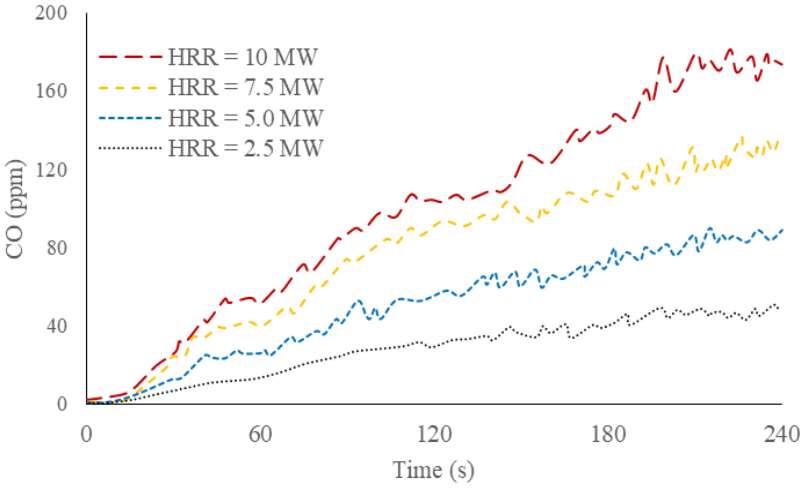

Fig. 8. The variations of CO concentration vs. time under the carriage ceiling for different HRRs

In order to analyze different critical conditions in the train carriages during the subway tunnel fire, the profiles of temperature and CO concentration are plotted at the other carriages with the fixed HRR.

The under-ceiling temperature versus time plot (Appendix Fig (g)) shows that the first and second carriages experience a dangerous state associated with high temperature after 110 and 120s of fire ignition, respectively. In contrast, the temperature of the two other carriages is lower. In addition, temperature increment for the first and second carriages are higher than other carriages after 60 s of fire ignition.

CO concentration increases over time at all carriages; however, a higher level of concentration occurs at the first and second carriages (Appendix Fig (h)), In other words, closer carriages to the fire source involve higher CO concentration and better entrainment of the fresh air into the smoke plume is reported for lower CO concentration. However, the CO concentration variation is linked to the velocity changes at different carriages shown (Appendix Fig (i)). This figure shows that slightly larger velocities have remarkable impacts on the declining procedure of CO concentration for each carriage. Fluctuating behavior of velocity profile during simulation is related to the open doors and windows of carriages. Simulation outputs are briefly listed in (Table 4) to attain a better view of two carriages with unsafe conditions in the subway tunnel fire.

6. Conclusions

In this paper, numerical simulation of a full-scale subway tunnel fire with a train is performed to analyze the effect of fire distance and heat release rate on the vertical and under-ceiling temperature and CO concentration. The governing equations of the subway fire are solved by FDS. Simulation results show that fire with a fixed position leads to high temperature at the first and second carriages in terms of unsafe condition. Also, the temperature beneath the ceiling shows higher values due to the lower entrainment of fresh air above the windows and doors. Furthermore, a higher CO concentration occurs in the carriages closer to the fire. Untenable temperature conditions are reported for the fireplaces near the carriages. The distribution of vertical CO concentration and velocity is highly related together in all cases. Indeed, a small increase in the velocity causes faster movement of the smoke flow, and lower CO concentration.

Two fire heat release rates of fire led to critical temperature at the first and second carriages for the nearest fire position to the train. HRR decrement is more effective than carriage position for a fixed fire location to get the maximum temperature in carriages, and the delaying time is higher.

Funding

This research did not receive any specific grant from agencies in the public, commercial, or not-for-profit sectors.

Table 4. Reported results of numerical simulation for the subway fire

Carriage No.	Fire location (m)	Maximum T (℃)	Maximum CO (ppm)	Reported time (s)	HRR (MW)
1	80	113.2	173.1	110	10
1	80	101.6	131.9	150	7.5
2	80	90.3	152.2	120	10
2	80	81.4	109.8	162	7.5
3	80	80.2	128	240	10
3	80	62.4	83.6	240	7.5
4	80	67.8	138	240	10
	80	44.1	63.2	240	7.5

References

[1] Hong WH. The progress and controlling situation of Daegu Subway fire disaster. Fire Safety Science. 2004;6: s-5.

[2] Meng N, Hu L, Wu L, Yang L, Zhu S, Chen L, Tang W. Numerical study on the optimization of smoke ventilation mode at the conjunction area between tunnel track and platform in emergency of a train fire at subway station. Tunnelling and Underground Space Technology. 2014 Feb 1;40:151-9.

[3] Wei T, Zhao W, Zong R. Analytical study of wall factor on the ceiling temperature distribution in the far field for tunnel fires. Journal of Wind Engineering and Industrial Aerodynamics. 2017 Dec 1;171:196-201.

[4] Zhong W. Study on smoke flow characters and management in subway station fire. Hefei: University of Science and Technology of China. 2007.

[5] Li YZ, Ingason H, Lönnermark A. Fire development in different scales of train carriages. In11th International Symposium on Fire Safety Science 2014 (pp. 302-315).

[6] Ingason H. Model scale railcar fire tests. Fire safety journal. 2007 Jun 1;42(4):271-82.

[7] Alarie Y. Toxicity of fire smoke. Critical reviews in toxicology. 2002 Jan 1;32(4):259-89.

[8] Chen LF, Hu LH, Tang W, Yi L. Studies on buoyancy driven two-directional smoke flow layering length with combination of point extraction and longitudinal ventilation in tunnel fires. Fire Safety Journal. 2013 Jul 1;59:94-101.

[9] Ji J, Guo F, Gao Z, Zhu J, Sun J. Numerical investigation on the effect of ambient pressure on smoke movement and temperature distribution in tunnel fires. Applied Thermal Engineering. 2017 May 25;118:663-9.

[10] Wu F, Zhou R, Shen G, Jiang J, Li K. Effects of ambient pressure on smoke back-layering in subway tunnel fires. Tunnelling and underground space technology. 2018 Sep 1;79:134-42.

[11] Cong W, Shi L, Shi Z, Peng M, Yang H, Zhang S, Cheng X. Effect of train fire location on maximum smoke temperature beneath the subway tunnel ceiling. Tunnelling and Underground Space Technology. 2020 Mar 1;97:103282.

[12] Peng M, Cheng X, Cong W, Yuen R. Experimental investigation on temperature profiles at ceiling and door of subway carriage fire. Fire technology. 2021 Jan;57(1):439-59.

[13] Peng M, Cheng X, He K, Cong W, Shi L, Yuen R. Experimental study on ceiling smoke temperature distributions in near field of pool fires in the subway train. Journal of Wind Engineering and Industrial Aerodynamics. 2020 Apr 1;199:104135.

[14] Meng N, Wang Q, Liu Z, Li X, Yang H. Smoke flow temperature beneath tunnel ceiling for train fire at subway station: Reduced-scale experiments and correlations. Applied Thermal Engineering. 2017 Mar 25;115:995-1003.

[15] Weng MC, Yu LX, Liu F, Nielsen PV. Full-scale experiment and CFD simulation on smoke movement and smoke control in a metro tunnel with one opening portal. Tunnelling and underground space technology. 2014 May 1;42:96-104.

[16] Lei W, Li A, Tai C. The effect of heat release rate on the environment of a subway station. Procedia Engineering. 2017 Jan 1;205:3717-20.

[17] Yuan Z, Lei B, Bi H. The effect of fire location on smoke temperature in tunnel fires with natural ventilation. Procedia Engineering. 2015 Jan 1;121:2119-24.

[18] Ji J, Zhong W, Li KY, Shen XB, Zhang Y, Huo R. A simplified calculation method on maximum smoke temperature under the ceiling in subway station fires. Tunnelling and Underground Space Technology. 2011 May 1;26(3):490-6.

[19] Sojoudi A, Afshin H, Farhanieh B, Saha S. Large eddy simulation of smoke flow in a real road tunnel fire using FDS. International Conference on Computational Methods 2012 (pp. 1-8). Queensland University of Technology.

[20] Sojoudi A, Afshin H, Farhanieh B. An analysis of carbone monoxide distribution in large tunnel fires. Journal of Mechanical Science and Technology. 2014 May;28(5):1917-25.

[21] Sojoudi AT, Afshin HO, Farhanieh BI. Comparative Study of Carbone Monoxide

and Temperature Vertical Distribution in Tunnel Fires. Journal of Solid and Fluid Mechanics. 2015 Dec 22;5(4):1-3.

[22] Sojoudi A, Afshin H, Farhanieh B. Numerical Study of Carbon Monoxide and Temperature Distribution in Tunnel Fires Employing Air Curtain. Journal of Solid and Fluid Mechanics. 2015 Sep 23;5(3):235-46.

[23] MO SJ, Li ZR, Liang D, Li JX, Zhou NJ. Analysis of smoke hazard in train compartment fire accidents base on FDS. Procedia Engineering. 2013 Jan 1;52:284-9.

[24] Zisis T, Vasilopoulos K, Sarris I. Numerical Simulation of a Fire Accident in a Longitudinally Ventilated Railway Tunnel and Tenability Analysis. Applied Sciences. 2022 Jun 2;12(11):5667.

[25] Zhu Y, Wang Y, Zhou X. Numerical Modelling and Prediction of the Train-induced Smoke Control in Tunnel Fire. InIOP Conference Series: Materials Science and Engineering 2018 Oct 1 (Vol. 423, No. 1, p. 012019). IOP Publishing.

[26] Cong W, Shi L, Shi Z, Peng M, Yang H, Cheng X. Numerical study on the ceiling gas temperature in a subway train with different fire locations. InBuilding Simulation 2022 Apr (Vol. 15, No. 4, pp. 549-560). Tsinghua University Press.

[27] Liu C, Zhong M, Tian X, Zhang P, Li S. Study on emergency ventilation for train fire environment in metro interchange tunnel. Building and environment. 2019 Jan 1;147:267-83.

[28] Teodosiu CI, Kubinyecz VF. Numerical Study on the Impact of Platform Screen Doors in a Subway Station with a Train on Fire. Applied Sciences. 2022 Aug 19;12(16):8296.

[29] Kong J, You W, Deng E, Li H. Study of the evolution mechanism of multi-window carriage fire under longitudinal ventilation in a metro tunnel. Tunnelling and Underground Space Technology. 2022 Sep 1;127:104618.

[30] Ren F, Shi C, Li J, Che H, Xu X. Numerical study on the flow characteristics and smoke temperature evolution under double fires condition with a metro train in tunnel. Tunnelling and Underground Space Technology. 2021 Aug 1;114:103943.

[31] Li YZ. CFD modelling of fire development in metro carriages under different ventilation conditions.

[32] McGrattan K, Hostikka S, McDermott R, Floyd J, Weinschenk C, Overholt K. Fire dynamics simulator user's guide. NIST special publication. 2013 Sep;1019(6):1-339.

[33] Chow WK, Li YZ, Cui E, Huo R. Natural smoke filling in atrium with liquid pool fires up to 1.6 MW. Building and Environment. 2001 Jan 1;36(1):121-7.

[34] NFPA N. 130-Standard for Fixed Guideway Transit System. National Fire Protection Association. 2003.

[35] McGrattan KB, Forney GP, Floyd J, Hostikka S, Prasad K. Fire dynamics simulator (Version 5): User's guide. US Department of Commerce, Technology Administration, National Institute of Standards and Technology; 2005 Sep.

[36] McGrattan K, Hostikka S, McDermott R, Floyd J, Weinschenk C, Overholt K. Fire dynamics simulator technical reference guide volume 1: mathematical model. NIST special publication. 2013;1018(1):175.

[37] Gao Y, Zhu G, Gu S, Tao H, Zhao Y. Experimental and numerical studies on ceiling maximum smoke temperature and longitudinal decay in a horseshoe shaped. tunnel fire. Case studies in thermal engineering. 2018 Sep 1;12:134-42.

Appendix

The additional tables and diagrams of paper are listed.

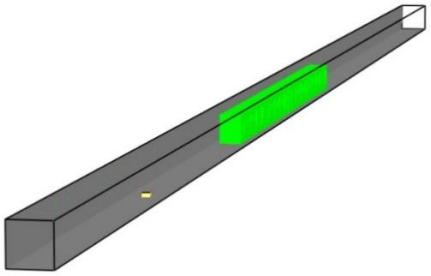

Fig. (a) Schematic of the simulated subway tunnel with train carriages by FDS

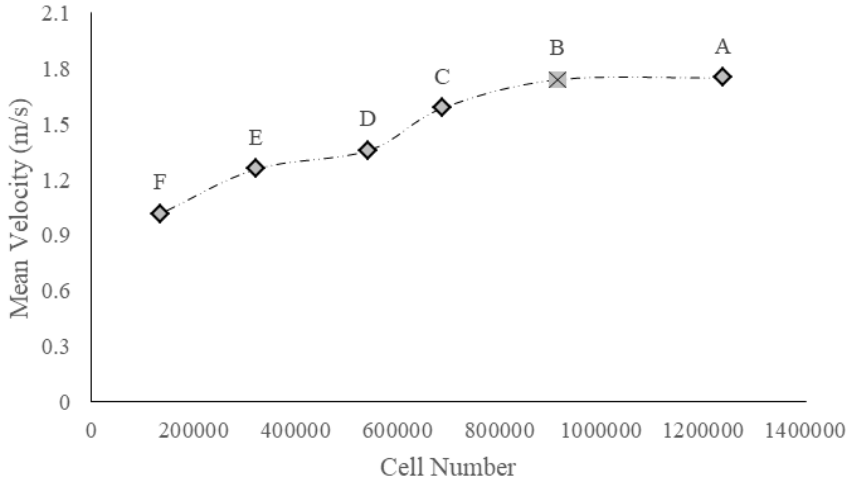

Fig. (b) Vertical distribution of the mean velocity for different grid systems at mid line of tunnel

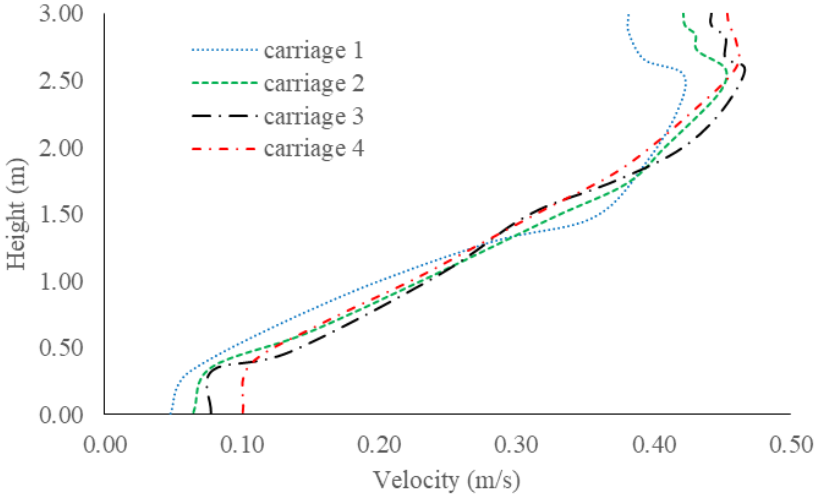

Fig. (c) Vertical velocity in the fixed fire position

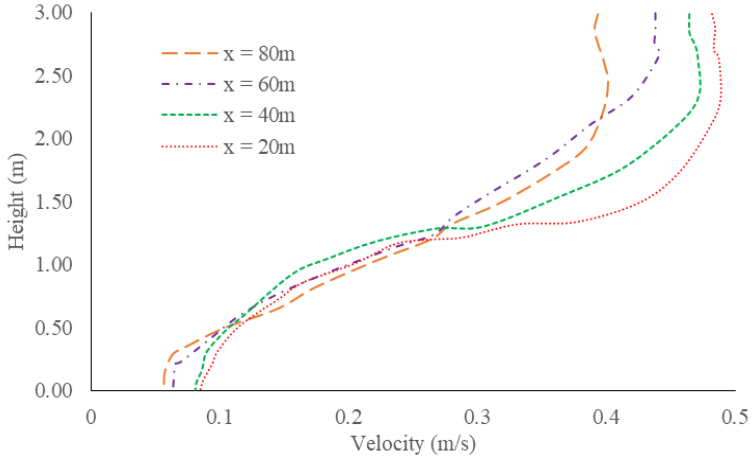

Fig. (d) Vertical velocity profile for different fireplaces

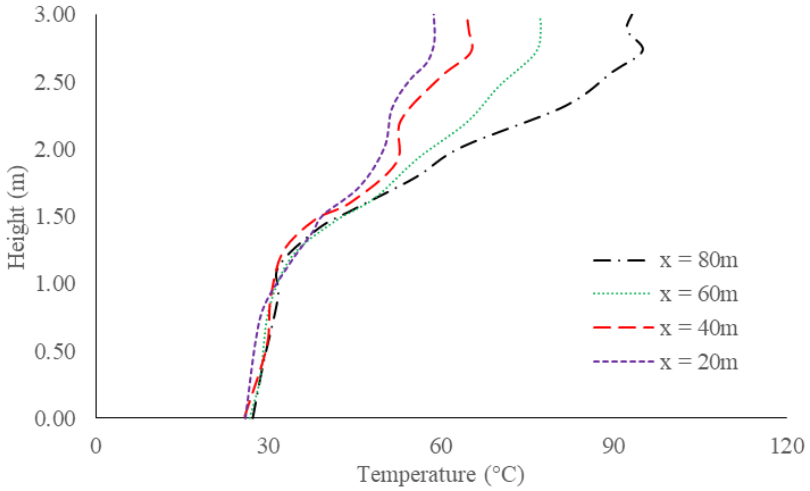

Fig. (e) Temperature profile vs. carriage height for different fireplaces

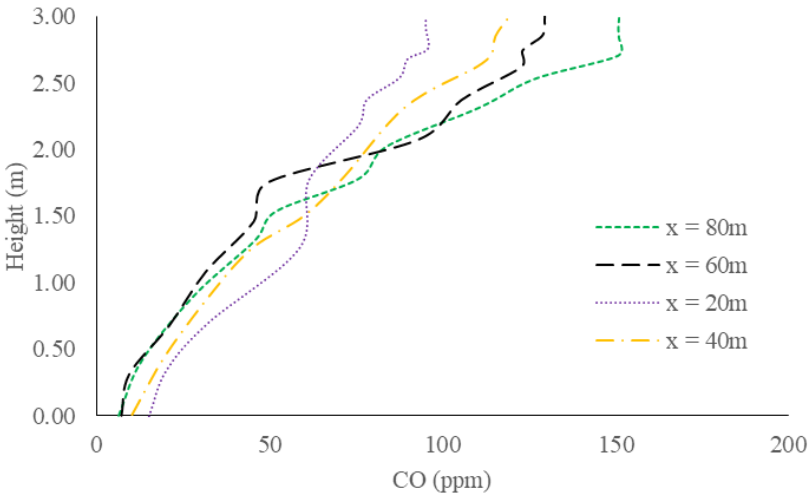

Fig. (f) CO concentration vs. carriage height for different fireplaces

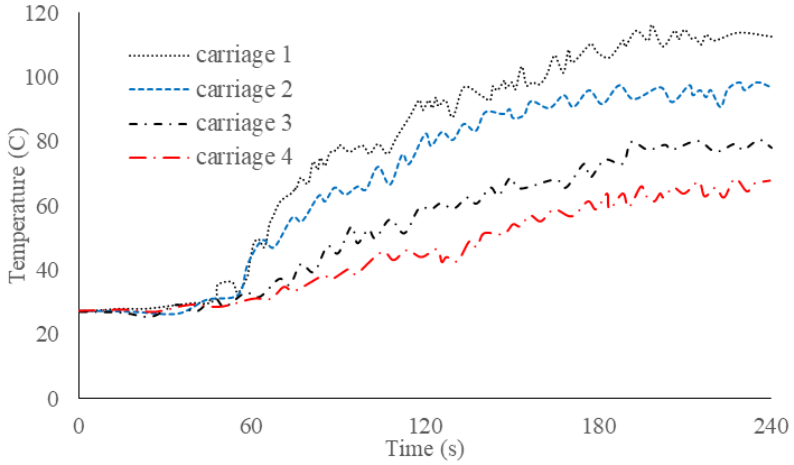

Fig. (g) The variations of under-ceiling temperature vs. time for different carriages

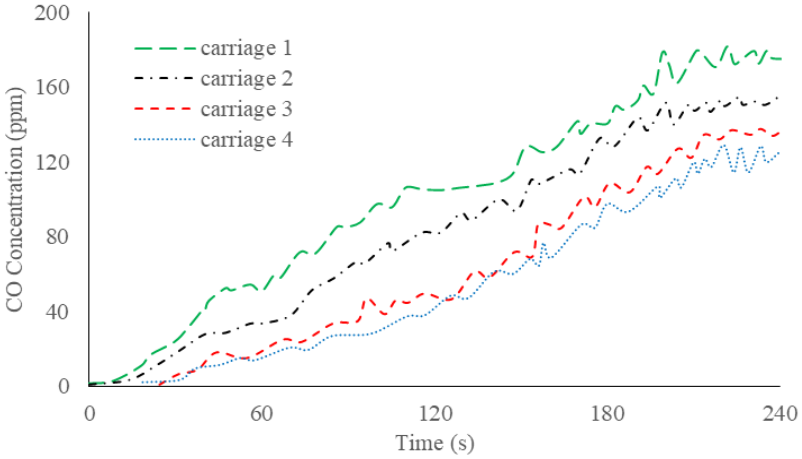

Fig. (h) The variations of under-ceiling CO concentration vs. time for different carriages

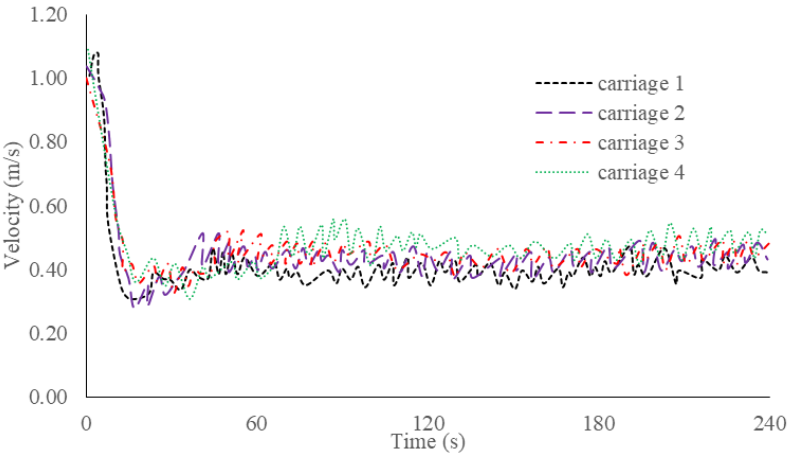

Fig. (i) The under-ceiling velocity variations vs. time for different carriages